

Bismuth nanowire arrays: Synthesis and galvanomagnetic properties

J. Heremans and C. M. Thrush

Delphi Automotive Systems Central Research and Development, Warren, Michigan 48090-9055

Yu-Ming Lin, S. Cronin, and Z. Zhang

Department of Physics, Massachusetts Institute of Technology, Cambridge, Massachusetts 02139-4307

M. S. Dresselhaus

*Department of Physics, Massachusetts Institute of Technology, Cambridge, Massachusetts 02139-4307
and Department of Electrical Engineering and Computer Science, Massachusetts Institute of Technology,
Cambridge, Massachusetts 02139-4307*

J. F. Mansfield

Department of Materials Science, University of Michigan, Ann Arbor, Michigan 48109-2143

(Received 21 June 1999; revised manuscript received 17 September 1999)

This paper reports galvanomagnetic properties of arrays of single-crystal bismuth nanowires, with diameters of 7 to 200 nm, embedded in an amorphous porous anodic alumina matrix. A sample preparation technique is described that makes it possible to obtain nanowires with diameters below 10 nm. The wires are single crystals, with their long axes oriented in the bisectrix/trigonal plane, about 19° from the bisectrix axis. The temperature dependence ($1.4 \text{ K} \leq T \leq 300 \text{ K}$) of the electrical resistance, longitudinal magnetoresistance ($0 \text{ T} \leq B \leq 5 \text{ T}$ with $1.4 \leq T \leq 75 \text{ K}$, and $0 \text{ T} \leq B \leq 1 \text{ T}$ with $80 \leq T \leq 300 \text{ K}$) and transverse magnetoresistance ($0 \text{ T} \leq B \leq 5 \text{ T}$ with $1.4 \leq T \leq 75 \text{ K}$) of the nanowires are given. The results extend previous work to wires of narrower diameter, and confirm the existence of the semimetal-semiconductor phase transition seen in the magnetoresistance. The data are discussed qualitatively in terms of the interplay between the electron cyclotron radii, electron scattering on the wire walls, size-induced energy level quantization, and the transfer of carriers between the different carrier pockets of the Fermi surface. Nanowires of Bi are theoretically predicted to have a much higher thermoelectric figure of merit than bulk Bi.

INTRODUCTION

The galvanomagnetic transport properties of nanowires of the semimetal Bi have been the subject of numerous studies spanning decades,¹ for a number of reasons. Firstly, the electron mean free path in bulk Bi can be on the order of a millimeter² at liquid helium temperatures, and this results in strong ballistic effects.³ Secondly, the electrons in Bi have a very small effective mass. This results in a large spatial extension of the electron wave function, which increases the effects of quantum confinement. Thirdly, the electron density is 10^5 times smaller at liquid helium temperatures than in conventional metals, resulting in a relatively large resistivity, in spite of the long mean-free path. Therefore resistance anomalies such as localization effects^{4,5} are enhanced. Finally, it has been calculated that Bi nanowires should have a very much enhanced thermoelectric figure of merit.⁶ Early measurements⁷ of the thermoelectric power of 200-nm nanowires have shown consistency between the diffusion thermopower and the Fermi energies obtained from Shubnikov-de Haas (SdH) oscillations.

Single-crystal filaments of Bi have been prepared with diameters in the micron range 20 years ago,¹ and diameters down to 200 nm have been achieved by high-pressure casting from the liquid phase.⁸ Several measurements of galvanomagnetic properties of Bi nanowires have been published.^{8,9} In particular an anomaly in the temperature dependence of the resistivity⁸ was interpreted as a possible de-

crease in diffuse scattering at the wire walls as the electron wave function becomes one-dimensional. Consistent with the theory published by Chambers,¹⁰ the longitudinal magnetoresistance shown by Brandt *et al.*⁹ at 4.2 K is positive at low magnetic fields, but above a critical field, the resistance decreases as the cyclotron orbit becomes smaller than the wire radius and boundary scattering is decreased. A detailed study¹¹ of the quantum oscillations obtained in the magnetoresistance of single-crystal Bi wires with diameters down to 100 nm obtained from the liquid phase has revealed the existence of two types of quantum oscillations, those due to “bulk” Bi at high-magnetic fields, and those due to quantum-size oscillations, as described by Dingle.¹² The quantum-size oscillations occur at a low-magnetic field, where the cyclotron radius r_c is smaller than the sample radius, and the electron wavefunction is thus confined by the sample walls.

More recently,^{13,14} porous alumina host materials have been used for the preparation of Bi nanowires. The pores were filled with liquid Bi by a similar high-pressure technique and the resulting solid Bi wires are single crystals with their long axis oriented in the same direction as those of the Russian work.^{9,11} Magnetoresistance measurements have shown that a semimetal-to-semiconductor transition takes place as the wire diameter is decreased from 100 to 65 nm. In the high-pressure liquid technique, the pressure needed to force the liquid Bi into the pores is inversely proportional to the pore diameter.⁸ Therefore, the smallest diameter single-

TABLE I. Dimensions of the pores in the alumina host materials used, and electrical resistance R at 300 K in zero-magnetic field of the Bi nanowire samples.

Sample	Average wire diameter d	Average spacing between wires	$R(300)$
	(nm)	(nm)	(Ω)
BiW09 and BiW11	200	400	404
BiJ1	70 ± 10	160	340
BiJ4	48 ± 6	116 ± 6	168
BiJ2	36 ± 5	75	1593
BiJ5	28 ± 3	45 ± 4	2528
BiY15	7 ± 2	15 ± 4	4105

crystal sample reportedly¹³ prepared from a melt is 65 nm.

In this paper we describe a vapor-phase method that does not rely on pressure to insert the host material into the pores of a host material, and can therefore in principle be generalized to create nanowire arrays of metals and semiconductors of much smaller diameters. We then report structural and galvanomagnetic properties of Bi nanowires with diameters ranging from 200 to 7 nm.

EXPERIMENT

For this study, we prepared nanowire arrays of Bi in porous amorphous alumina templates with six different wire diameters d . The samples are described in Table I. Samples based on templates with 200-nm diameter pores were prepared using commercially available Whatman Anodisc alumina as the host material; the host material or template for the other samples was prepared by anodic oxidation of aluminum metal.¹⁴ All host templates come as flat free-standing plates of alumina, about $50 \mu\text{m}$ thick, which contain an array of holes running parallel to each other from one face of the plate to the other. A plan-view scanning electron microscopy (SEM) image of the array with the narrowest pores is shown in Fig. 1.

A new vapor-phase technique, in a diffusion pumped, liquid nitrogen trapped vacuum evaporator with a base pressure of about 5×10^{-7} torr, is used to fill the pores of the alumina. The technique is schematically illustrated in Fig. 2. An alumina crucible inserted in a simple resistively heated oven

(R. D. Mathis Company #CH-10 with an alumina crucible 13-mm OD) is filled with 99.9999% bismuth, to approximately one quarter full. The porous alumina plate is placed over the crucible, totally covering its mouth. If the porous alumina plate has a diameter smaller than the crucible, a molybdenum washer is inserted between the crucible lip and the porous plate. A molybdenum or graphite top plate 0.5 mm thick is then placed on top of the porous alumina plate. This top plate acts as a heat sink and establishes a temperature gradient across the porous alumina plate between the top plate and the heated Bi oven. A tungsten clip can be used to hold the whole assembly in place. A small piece of Bi is added on top of the top plate. The heater containing the bismuth metal is then slowly heated. At lower crucible temperature, the bismuth condenses on the bottom of the alumina and forms droplets. As the heater temperature increases, the porous alumina plate and the top plate heat up to a temperature ($T \approx 400\text{--}500^\circ\text{C}$) where bismuth has a high vapor pressure. At this temperature bismuth re-evaporates from the bottom of the porous plate and starts penetrating into the pores until it condenses onto the top plate. The heat is further increased until the bismuth vapor passes through the porous alumina and evaporates from the top end of the alumina plate, leaving nothing behind in the pores: this cleans the porous alumina. When the small piece of Bi on top of the top plate has evaporated, a slow cool-down phase is initiated. Because the top plate is cooler than the crucible, Bi starts condensing at the topside of the porous plate first.

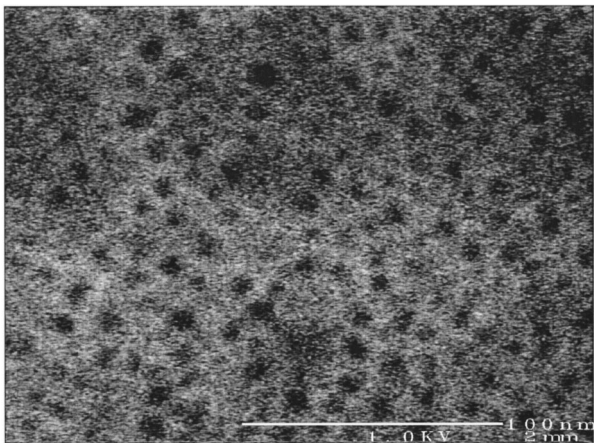


FIG. 1. Scanning electron micrograph of an anodic alumina template with 7 ± 2 -nm pores.

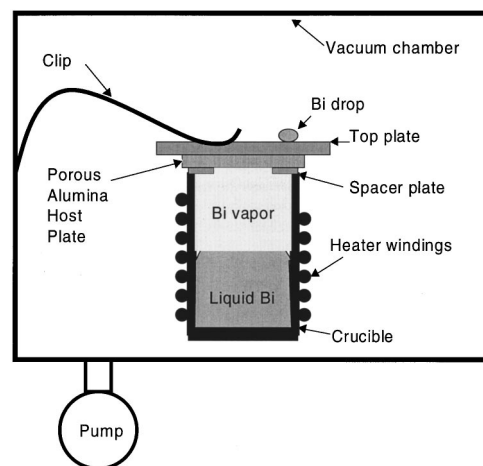


FIG. 2. Schematic diagram of the vacuum chamber containing the sample-preparation technique.

Single-crystal (as will be shown later) wires of bismuth grow through the pores of the alumina from the topside downwards. Once the porous plate's bottom side has reached a temperature below 271 °C, where bismuth is a solid, the process is finished. The total time of the process from heatup to the end of the controlled cool down is approximately 15 min, once the chamber has achieved its base pressure. The study of the different stages of the formation of bismuth wires described above was conducted by halting the process at the various stages, and analyzing the results under a microscope.

A cross-sectional scanning electron microscope (SEM) image of a 200-nm Bi nanowire array is shown in Ref. 4, and similar images were taken on most nanowire arrays. An aqueous solution of 5% by volume of H_3PO_5 and 45 g/liter of CrO_3 acts as a selective etch, dissolving the Al_2O_3 template while leaving the Bi nanowires intact. At room temperature, this process takes 2 to 48 h, depending on the amount of Al_2O_3 to be dissolved. It is thus possible to prepare transmission electron microscopy samples of freestanding wires on which lattice fringes can be observed. These studies reveal that the Bi nanowires are single crystals throughout their length. X-ray diffraction data taken on the BiJ1 and BiJ4 wires (see Table I) are identical to those reported on liquid phase-prepared wires.¹³ A comparison of the peak intensities to those of polycrystalline Bi show that 85 to 95% of the samples have the longitudinal axes of the wires oriented along the $(h,k,l)=(1,0,1)$ direction. In the rhombohedral [x =binary, y =bisectrix, z =trigonal] axis system, this indexes to $[x,y,z]=[0,0.949,0.315]$; the longitudinal axis of the Bi wires thus lies in the trigonal-bisectrix plane, 18.4° from the bisectrix axis, much the same direction as that of the wires studied in the Russian work.^{9,11} The main peak indexes to a d spacing of 1.8688 Å, very close to the (2,0,2) peak in polycrystalline Bi ($d=1.8686$ Å), which implies that there is very little strain in the samples. As will be seen in the magnetoresistance data, Shubnikov-de Haas (SdH) oscillations are observed in the semimetallic samples. As the Fermi surface of Bi consists of three electron and one hole pocket, the SdH periods in bulk Bi for the magnetic field aligned with the $[0, 0.949, 0.315]$ axis are quite close to those along the $[0,0,1]$ axis. To resolve any ambiguity, Kikuchi patterns were obtained in the reflection mode in a SEM on one sample (BiW11). While it was not possible to resolve the orientation from these patterns, which were very faint due to the low scattering volume, it was clear that the patterns did not show the threefold symmetry consistent with a trigonal wire orientation. A study of the SdH oscillations on 200-nm wires prepared from 99.9999% pure Bi (Ref. 7) shows a difference between electron and hole densities on the order of $3.8 \times 10^{17} \text{ cm}^{-3}$. Since the sample must be charge neutral, this number can be viewed as a rough measurement of the density of ionized impurities in the wires.

Two samples from each growth of the Bi nanowire arrays in each porous alumina template were mounted for resistance and magnetoresistance measurements as a function of temperature and magnetic field. The measurements were made using two electrical probes, attached to the bottom and top surfaces of the Bi-filled anodic alumina plates with silver epoxy and silver paint. The direction of current was along the long axis of the wires. Each of the probes contacted an area of about 1 mm², which contained many Bi nanowires in

parallel. The value of the room-temperature resistance of the samples at zero magnetic field are reported in Table I. Unfortunately, only a fraction of the pores are filled and not all the Bi nanowires fully fill the length of the pore (see Fig. 1 in Ref. 4). It is therefore impossible to estimate the absolute value of the resistance of one nanowire for any of the wire diameters that were studied, and only relative data, specifically resistance values normalized to 300 K, and magnetoresistance data relative to the value at zero-magnetic field, are reported, as in Ref. 4. The sample-to-sample repeatability of the relative data was very good for samples of similar diameters. Only the data on one sample of each diameter are reported in this paper. A second reason to only report relative data is the fact that the measurements are essentially two-wire measurements, which may contain a contribution from contact resistances. True four-wire measurements on single-Bi nanowires are highly desirable, but they require lithography at the nm scale and are technologically difficult to achieve. We estimate that the relative data presented here contain a contribution from variations in the contact resistances that is likely to be on the order of 1%. We measured the contact resistance between silver epoxy, silver paint, and bulk Bi to be of the order of a fraction of an Ohm over the temperature range studied. The SEM image in Ref. 4 illustrates that the imbedded nanowires prepared by the vapor-phase technique are terminated by balls of bulk Bi on both faces of the anodic alumina plate, and it is to these balls that the silver-containing polymers make contacts. Given the sample resistance values reported in Table I and the temperature dependence reported later, a 0.1 to 1 Ω contact resistance is very small. In addition, we have repeated the measurements on a 40-nm diameter wire (similar to BiJ2) using Wood's metal as contact material, since this alloy is known to make excellent contacts to Bi. Again, the relative data obtained were very similar to those on sample BiJ2. For the two reasons stated, sample-to-sample repeatability and magnitude of the contact resistance, it is estimated that on vapor-grown nanowires, the error in the relative data due to contact resistances remains at the 1% level.

Each sample was first mounted in a liquid-He cryostat and the electrical resistance was measured from 1.4 to 75 K in a magnetic field $B(0 \text{ T} \leq B \leq 5 \text{ T})$ aligned both parallel and perpendicular to the long axis of the wires, yielding the longitudinal and transverse magnetoresistance data. The samples were then mounted in a liquid nitrogen cryostat and the resistance and longitudinal magnetoresistance were measured in the temperature range $77 \text{ K} \leq T \leq 300 \text{ K}$ (sometimes to 200 K) and in the field range $0 \text{ T} \leq B \leq 1 \text{ T}$. The alignment between the wire long axis and the longitudinal field was only controlled to within a few degrees, because balls of Bi metal were present on the sample faces and this made it difficult to mount the alumina plates perfectly flat. Self-balancing low-frequency ac bridges (Linear Instruments LR-400 or LR-700 bridges) were used to measure the sample resistances. The excitation voltages were varied from 20 μV to 2 mV, with no effect on the results; most traces reported in this paper were recorded at 200 or 600 μV excitation voltages.

RESULTS

Figure 3 shows the temperature dependence of the resistance of each sample, normalized to the resistance at 300 K.

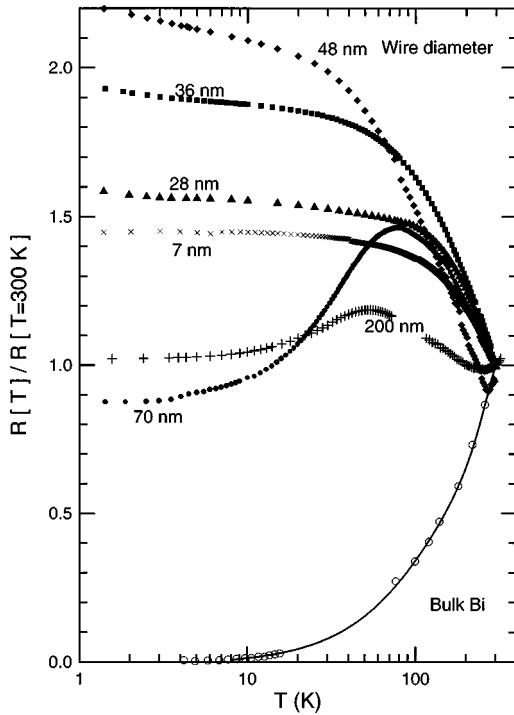


FIG. 3. Resistance at zero-magnetic field of Bi nanowire arrays, as a function of temperature, normalized to the resistance at 300 K.

Figures 4 through 9 show the magnetic-field dependence between 1.4 and 70 K of the longitudinal (a) and transverse (b) magnetoresistance of the six nanowire arrays that were studied. The magnetoresistance is normalized to the resistance at zero field at each temperature. Both the longitudinal and the transverse magnetoresistances below 70 K are quadratic functions of the magnetic field at low field, specifically for $0 \leq B \leq 1$ T above 10 K and $B < 0.2$ T below 10 K. The longitudinal magnetoresistance at temperatures above 77 K and at fields below 1 T is also a quadratic function of magnetic field for every sample. Therefore, the magnetoresistance can be expressed by the coefficient A :

$$A = \frac{R(B, T) - R(0, T)}{R(0, T)} \frac{1}{B^2}, \quad (1)$$

which is shown as a function of temperature in Fig. 10 for the longitudinal magnetoresistance, and in Fig. 11 for the transverse magnetoresistance.

DISCUSSION

The temperature dependence of the resistivity of 99.9999% pure bulk Bi measured along the trigonal direction is shown in Fig. 3 for comparison. The electron density in pure Bi increases^{2,15,16} from $2.7 \times 10^{17} \text{ cm}^{-3}$ at liquid helium temperatures to $3 \times 10^{18} \text{ cm}^{-3}$ at 300 K. On the other hand, the mobility^{2,15,16} decreases by 3.5 orders of magnitude over this temperature range, so that the temperature dependence of the mobility dominates over that of the electron density.

The band structure of Bi consists of three degenerate ellipsoidal electron pockets at the L points of the Brillouin zone, and one ellipsoidal hole pocket at the T point. The

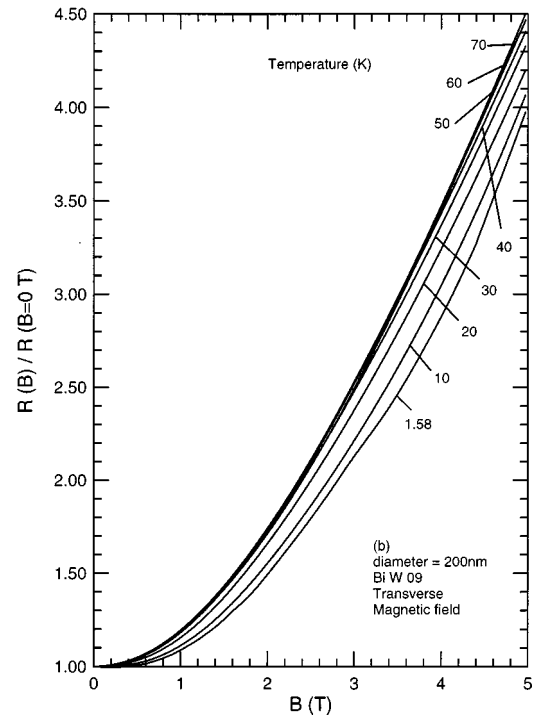
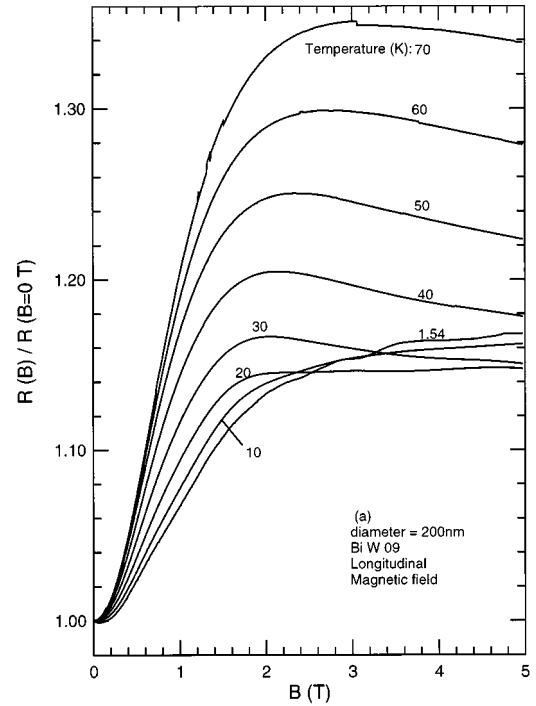


FIG. 4. Magnetic-field dependence of the longitudinal (a) and transverse (b) magnetoresistance of the 200-nm diameter Bi nanowire array, normalized to the resistance at zero field at the same temperature.

effective mass tensors for the electrons \mathbf{m}_e and holes \mathbf{m}_h in the trigonal axis system $[x, y, z]$ and normalized to the free electron mass, is given at 4 K by¹⁷

$$\mathbf{m}_e = \begin{bmatrix} 0.00119 & 0 & 0 \\ 0 & 0.263 & -0.0274 \\ 0 & -0.0274 & 0.00516 \end{bmatrix}, \quad (2a)$$

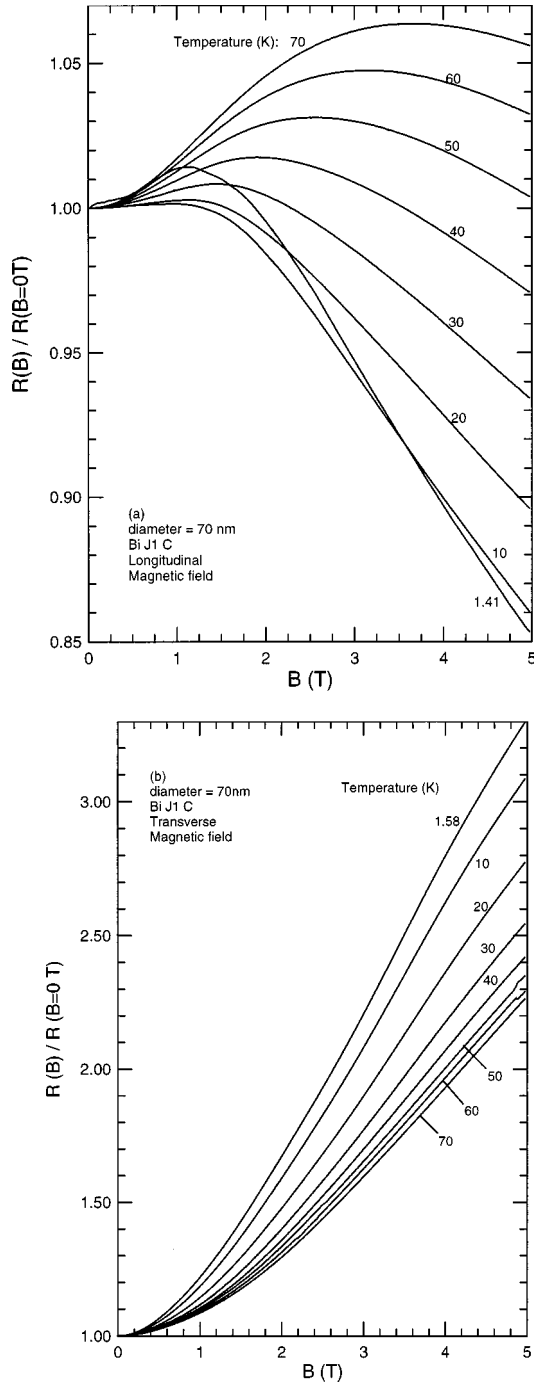


FIG. 5. Magnetic-field dependence of the longitudinal (a) and transverse (b) magnetoresistance of the 70-nm diameter Bi nanowire array, as in Fig. 4.

$$\mathbf{m}_h = \begin{bmatrix} 0.064 & 0 & 0 \\ 0 & 0.064 & 0 \\ 0 & 0 & 0.69 \end{bmatrix}. \quad (2b)$$

Since the long axis of the wires is not along the trigonal direction, the degeneracy of the energy levels of the three electron pockets is lifted so that the subbands associated with the two ‘‘heavy electron’’ pockets lie below the respective subbands of the third, or ‘‘light electron’’ pocket. The electron effective masses along the wire axis $h = [0, 0.949, 0.315]$ are thus defined as

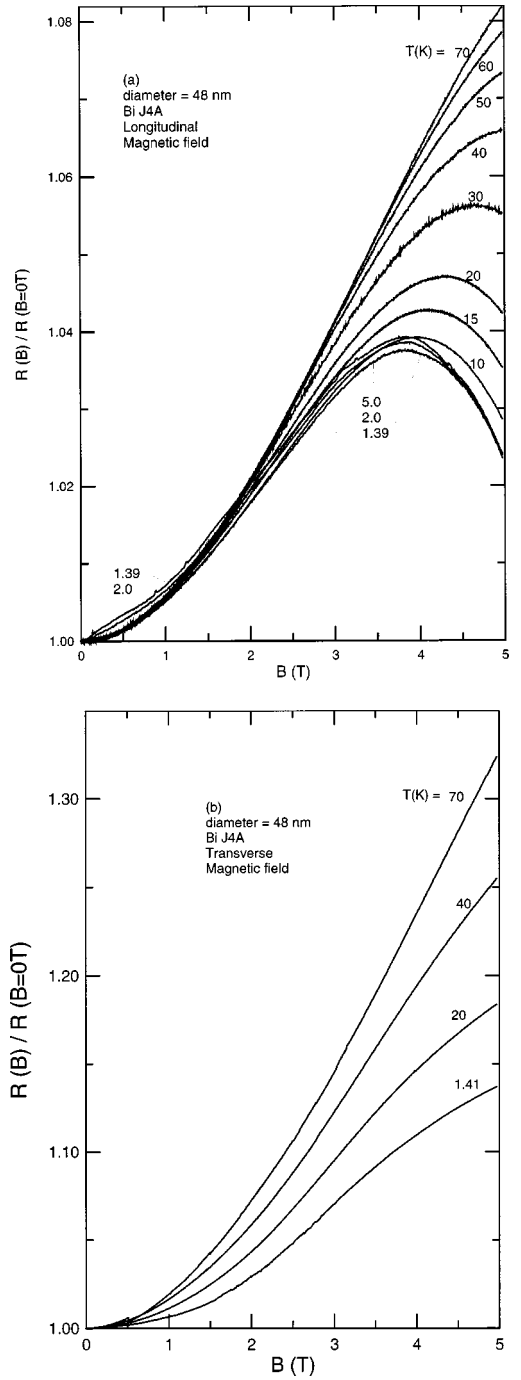


FIG. 6. Magnetic-field dependence of the longitudinal (a) and transverse (b) magnetoresistance of the 48-nm diameter Bi nanowire array, as in Fig. 4.

$$m_{leL} = h \cdot \mathbf{m}_e \cdot h^T \quad (3)$$

and

$$m_{leH} = k \cdot \mathbf{m}_e \cdot k^T, \quad (4)$$

where k is the vector h rotated by $\pm 120^\circ$. Similarly for holes

$$m_{lh} = h \cdot \mathbf{m}_h \cdot h^T. \quad (5)$$

The cyclotron orbit for each of these three pockets along h is an ellipse with an average cyclotron mass of

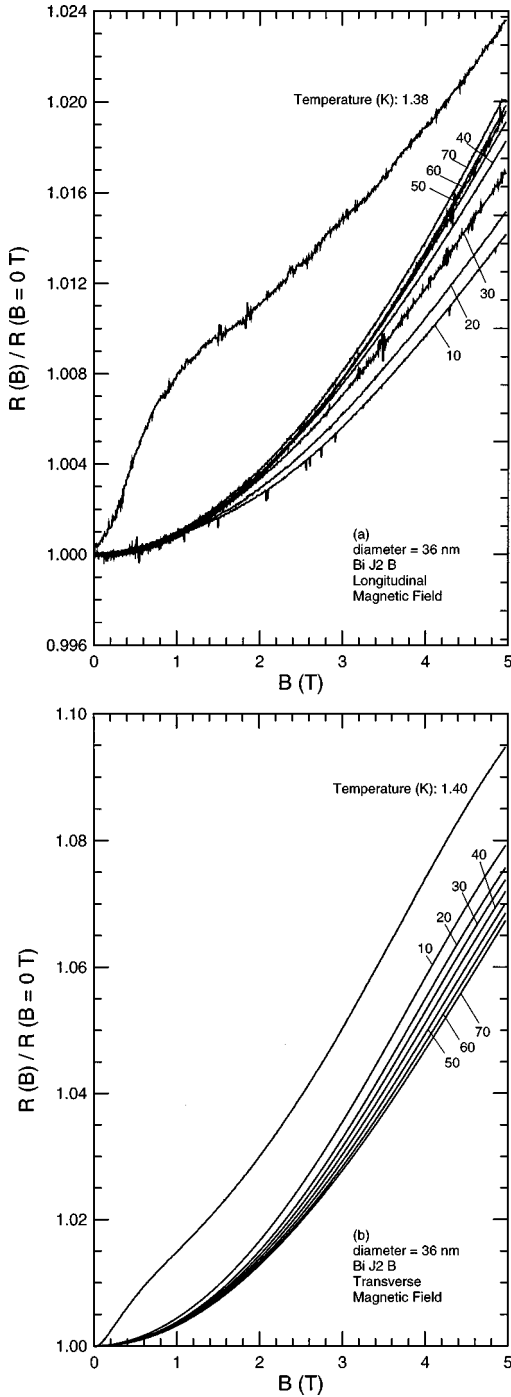


FIG. 7. Magnetic-field dependence of the longitudinal (a) and transverse (b) magnetoresistance of the 36-nm diameter Bi nano-wire array, as in Fig. 4.

$$m_{ceH} = \frac{\det(\mathbf{m}_e)}{m_{leH}}, \quad m_{ceL} = \frac{\det(\mathbf{m}_e)}{m_{leL}}, \quad m_{ch} = \frac{\det(\mathbf{m}_h)}{m_{lh}}. \quad (6)$$

Values for these masses are given in Table II. All the band structure parameters have temperature coefficients^{18,17} that come into play mostly at temperatures above 77 K and that need to be included in future, more quantitative calculations.

The formalism used for the effective mass tensors can be used for the mobility tensors, reported in the liquid-He range by Ref. 2 and from 77 to 300 K by Ref. 16. The mobilities,

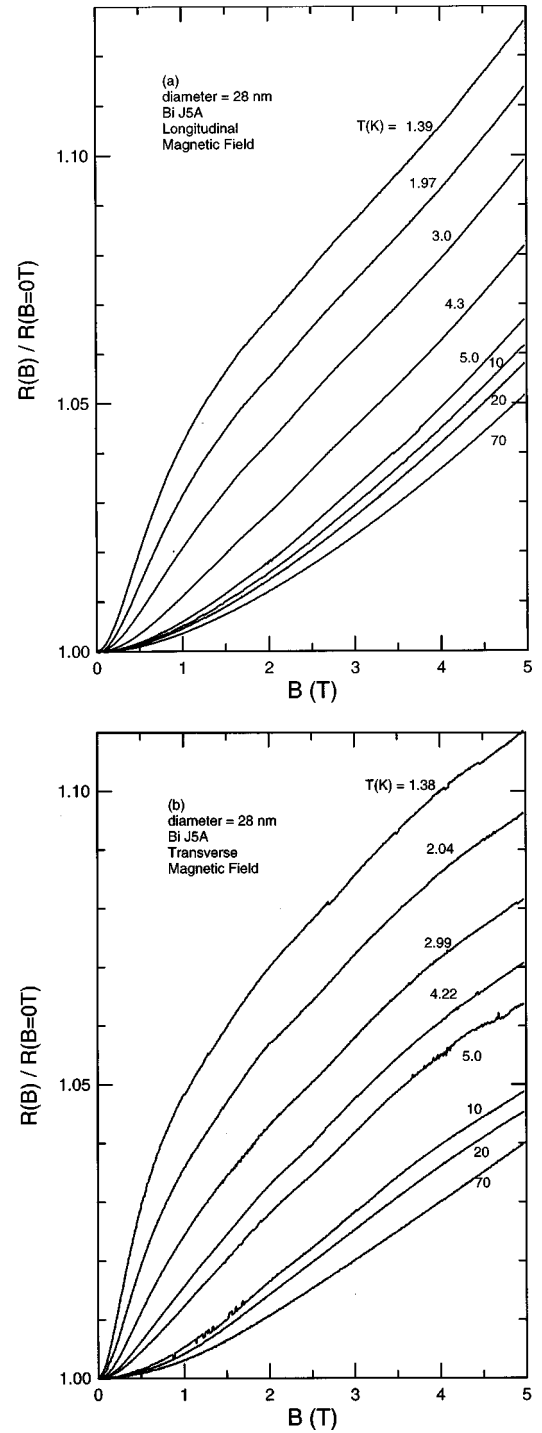


FIG. 8. Magnetic-field dependence of the longitudinal (a) and transverse (b) magnetoresistance of the 28-nm diameter Bi nano-wire array, as in Fig. 4.

noted for the light electrons $\mu_L(T)$, for the heavy electrons $\mu_H(T)$, and for the holes $\nu(T)$, are functions of the longitudinal masses. The mean-free paths (mfp), noted for the light electrons $\lambda_{eL}(T)$ and for the heavy electrons $\lambda_{eH}(T)$, and for the holes $\lambda_h(T)$, are given, as a function of mobility, by

$$\lambda = v_F \cdot \tau, \quad (7)$$

where v_F is the carrier velocity at the Fermi level, and can be expressed as a function of the Fermi energy, while the carrier relaxation time τ is deduced from the mobility. The electron-

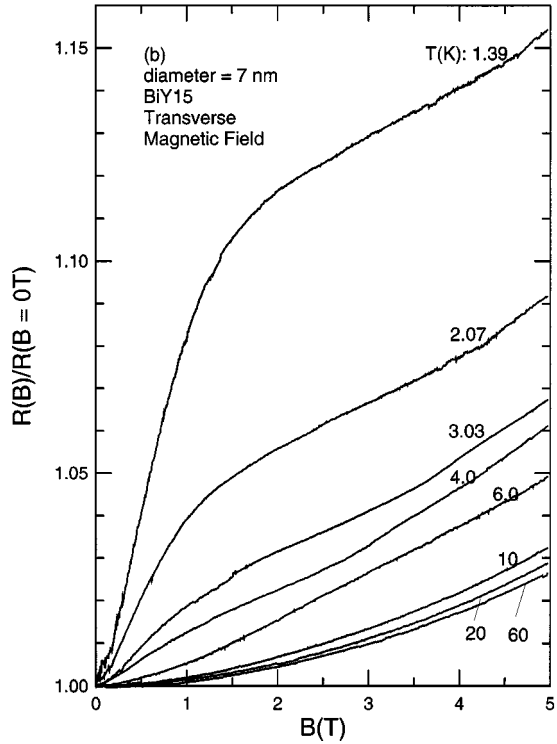
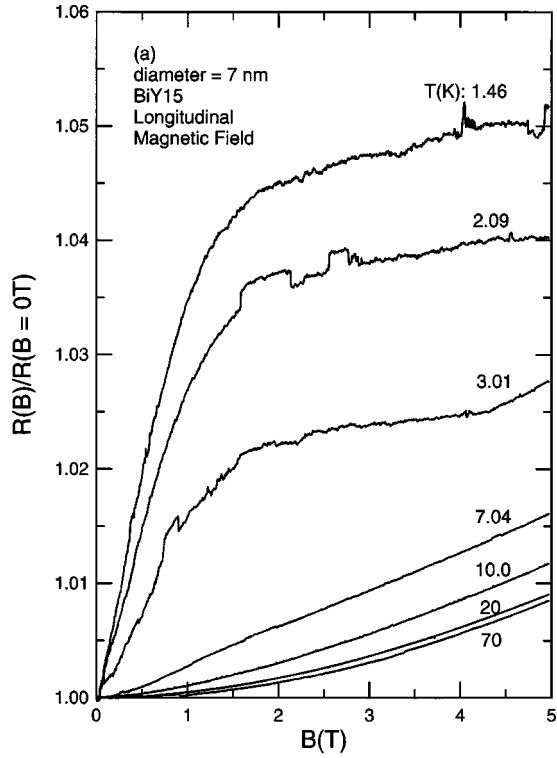


FIG. 9. Magnetic-field dependence of the longitudinal (a) and transverse (b) magnetoresistance of the 7-nm diameter Bi nanowire array, as in Fig. 4.

dispersion relation¹⁷ is strongly nonparabolic, which is expressed through the use of the quantities γ and γ' defined as a function of the electron energy E and the direct band gap at L point $E_g = 13.6$ meV by

$$\gamma = E \left(1 + \frac{E}{E_g} \right), \quad \gamma' = \left(1 + 2 \frac{E}{E_g} \right). \quad (8)$$

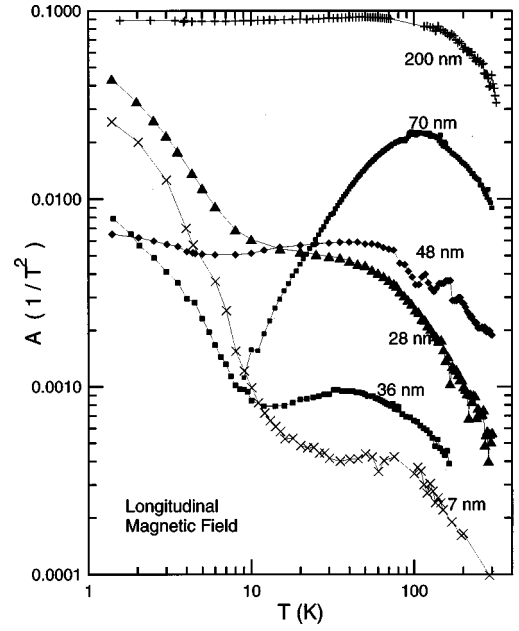


FIG. 10. Temperature dependence of the longitudinal magnetoresistance coefficient measured in the field range $0 \leq B \leq 1$ T at temperatures above 10 K and in the field range $0 \leq B \leq 0.2$ T below 10 K.

In this framework, the electron mean-free paths are given, as a function of mobility, by

$$\lambda_e = \frac{\mu}{q} (2m_{le}\gamma_{Fe})^{1/2}, \quad (9)$$

which applies for both heavy and light electrons, while the hole mfp is

$$\lambda_h = \frac{V}{q} (2m_{lh}E_{Fh})^{1/2}, \quad (10)$$

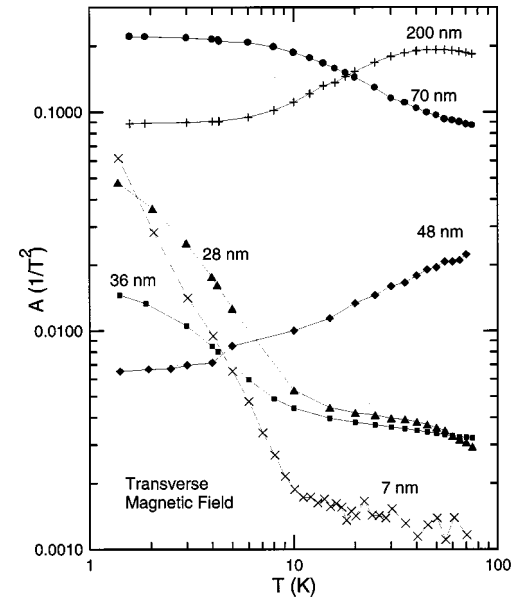


FIG. 11. Temperature dependence of the transverse magnetoresistance coefficient measured in the field range $0 \leq B \leq 1$ T.

TABLE II. Longitudinal and cyclotron effective masses, normalized to the free-electron mass, mean-free paths λ at room temperature and at 4.2 K, and cyclotron radii at a field of 1 T below 77 K along the nanowire axis for electrons and holes.

	Heavy electrons	Light electrons	Holes
Longitudinal mass	$m_{leH}=0.069$	$m_{leL}=0.221$	$m_{lh}=0.126$
Cyclotron mass	$m_{ceH}=0.00324$	$m_{ceL}=0.00181$	$m_{ch}=0.150$
$\lambda(4.2\text{ K})$	0.4 mm	0.1 mm	0.4 mm
$\lambda(300\text{ K})$	50–150 nm	45–130 nm	80 nm
$r_c(B=1\text{ T})$	80 nm	40 nm	135 nm

In the equations above, E_{Fh} is the hole Fermi energy, γ_{Fe} is the function (8) taken at the electron Fermi energy, and q is the electron charge. The mean-free paths can be calculated at 4.2 K from the mobility tensor elements, and the results are given in Table II. At room temperature the mfp value can be calculated using the temperature dependence of the effective Bohr magnetons along the bisectrix direction (close to the wire direction) from¹⁸ and of the Fermi energy from;¹⁷ however, there is considerable uncertainty about the value of m_{22} at 300 K,¹⁷ and thus about m_{leH} and m_{leL} . This is reflected in the ranges given for the mfp at room temperature. With these approximate numbers for the carrier mean free paths, it is now possible to separate the nanowires into two classes. In wires with diameters below about 45–80 nm, carrier scattering on the wire walls is expected to dominate transport at all temperatures. In wires with larger diameters d , there will be two temperature regimes: at temperatures below which the condition $\lambda=d$ holds, transport is also dominated by scattering on the walls, while at temperatures above that, acoustic phonon scattering is more important, similarly to the case of bulk Bi. The temperature dependence of the 70 and 200 nm wires, which belong to this second class, is nonmonotonic. This may be attributed to the existence of a distribution in wire diameters¹³ or to a temperature dependence of the specularly parameter of the scattering on the walls due to size quantization.⁸ In any event, this nonmonotonic temperature dependence has been observed earlier^{8,9,13} in wires of similar diameter. The mobility in the narrower wires is dominated by scattering on the walls, which is mostly temperature independent. The temperature dependence of the resistance, as shown in Fig. 3, then essentially reflects that of the electron density, which is reported in Fig. 12 and compared to pure Bi. A monotonic progression with decreasing diameter is observed in Fig. 12: the low-temperature residual carrier density increases with decreasing diameter. As the diameter decreases, the carrier density also becomes less temperature-dependent.

Turning now to the longitudinal magnetoresistance curves in Figs. 4 to 9, one observes that the magnetoresistance of the wires with diameters $d \geq 48$ nm starts positive at low field, but passes through a maximum and then decreases with increasing field. The longitudinal magnetoresistance of the thinner wires is monotonically positive. The positive magnetoresistance of Bi is due,² both in the longitudinal and in the transverse directions, to the strongly nonspherical Fermi surface and to the simultaneous presence of electrons and holes in the semimetallic regime. The amplitude of the magnetoresistance is, very roughly, proportional to the square of the

mobility. The nonmonotonic field dependence of the longitudinal magnetoresistance of the thicker wires has also been observed previously^{9,13} and is explained by Chambers¹⁰ in terms of the cyclotron radius r_c , of the wire. In the nonparabolic framework, the cyclotron radii are given, as a function of the average wavevector over the cyclotron orbit k_{cF} at the Fermi energy and the magnetic field B by

$$r_{ceL} = \frac{\hbar k_{FcL}}{q \cdot B} = \frac{1}{q \cdot B} (2m_{ceL} \gamma_{Fe})^{1/2} \quad (11)$$

for light electrons,

$$r_{ceH} = \frac{\hbar k_{FcH}}{q \cdot B} = \frac{1}{q \cdot B} (2m_{ceH} \gamma_{Fe})^{1/2} \quad (12)$$

for heavy electrons, and

$$r_{ch} = \frac{\hbar k_{Fch}}{q \cdot B} = \frac{1}{q \cdot B} (2m_{ch} E_{Fh})^{1/2} \quad (13)$$

for holes. The numerical values for bulk Bi at 4.2 K are also given in Table II. At low fields such that $r_c > d/2$, carriers scatter dominantly on the wire walls, and the resistance is high, yet since the mobility is not negligible, there is positive magnetoresistance. As the field increases above the value where $r_c = d/2$, scattering on the wall is much decreased, and the resistance value decreases because the mobility increases. This effect is partially counteracted by the increased magnetoresistance: the resistance curve in magnetic field thus will rejoin the curve for bulk Bi. The maximum magnetoresistance should very roughly occur at a magnetic field where

$$r_c = d/2. \quad (14)$$

From condition (14) and the relations (11)–(13) between the cyclotron radius and the average cyclotron wave vector k_{Fc} , the latter quantity can be deduced as a function of temperature for the samples which do display a maximum in longitudinal magnetoresistance. This is done in Fig. 13. The location of the maximum is extremely sensitive to the alignment between field and wire axis, especially in the very thin wires, and this alignment is difficult to control in the samples studied. A tilt in the sample results in an overestimation of the field at which the peak occurs, and thus an overestimation of k_{Fc} . Furthermore, the field at which the maximum magnetoresistance occurs depends on the absolute magnitude of the

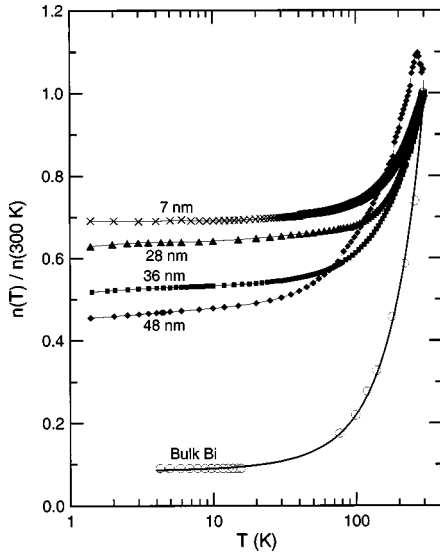


FIG. 12. Temperature dependence of the electron density in the narrower wires, normalized to 300 K. The curve for pure Bi is taken from Refs. 1 and 16. The values at high temperature of the curve for the 48-nm wire are not reliable, since the condition $\lambda > d$ is not valid there.

magnetoresistance, and relation (14) only very approximately defines that field. For those reasons, the absolute values in Fig. 13 are not precise. The temperature dependence of the effect is also affected by the temperature dependence of acoustic phonon scattering, which affects the absolute value of the magnetoresistance at high field ($r_c < d/2$) and therefore the position of the maximum. Finally, the measured values of k_{Fc} are really an average between the three carrier pockets. For comparison, the calculated values of k_{Fc} for the heavy and light electrons and for the holes in bulk Bi are also shown in Fig. 13, using the temperature dependence of the carrier density^{2,16} and assuming that the band structure has no temperature dependence below 77 K.^{17,18} A comparison between bulk and wires in Fig. 13 shows that the measurements on the 48- and 70-nm wires do give the right order of magnitude, but that there is more temperature dependence to the value of k_{Fc} in the wires than in the bulk. A more qualitative interpretation of the data was not carried out. The longitudinal magnetoresistance of the thinnest wires is also always positive, which implies that either the samples were tilted, or that the pores in the alumina are not straight to within a few diameters, or that the condition $r_c = d/2$ is never reached. In the latter case, only an upper limit can be given for $r_c(B = 5 \text{ T})$, which means that for the 36-nm wire, $k_{Fc} > 2.7 \times 10^8 \text{ m}^{-1}$ and for the 28-nm wire $k_{Fc} > 2.2 \times 10^8 \text{ m}^{-1}$.

Note that the low-field quadratic magnetic field dependence of the longitudinal magnetoresistance in the wires extends over a much larger field range (0.2 T below 10 K in the 200-nm wires) than in bulk Bi for which it extends only over about $2 \times 10^{-4} \text{ T}$ at liquid helium. This observation is consistent with the fact that the electron mobility is greatly reduced due to scattering on the wire walls. If the mean free path at 4.2 K of pure Bi is on the order of 0.4 mm (Table I) and on the order of 200 nm in the widest wire, the quadratic field range

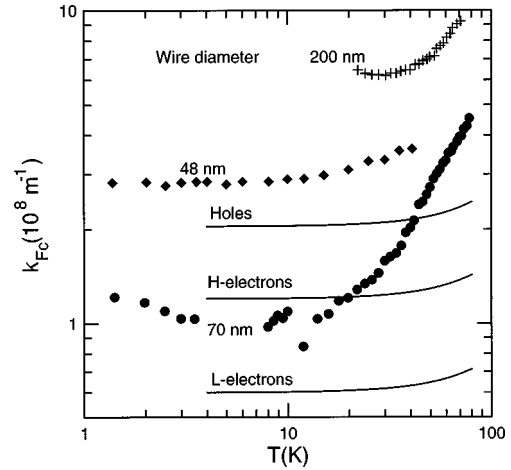


FIG. 13. Wave vector at Fermi energy, deduced from the positions of the maxima in longitudinal magnetoresistance, as a function of temperature. For comparison, the values calculated for pure Bi for light and heavy electrons and for holes in the direction perpendicular to the $[0,0.949,0.315]$ direction are given.

in the magnetoresistance of the wires is expected to be larger by about a factor of 2000, as observed.

The transverse magnetoresistance is a monotonically increasing function of field, consistently with the picture given for the longitudinal magnetoresistance. The transverse as well as the longitudinal magnetoresistance curves of the samples with 48, 36, 28, and 7 nm diameters show an additional ‘‘bump.’’ When one visually compares the shape of the MR curves at 1.4 K to those at 4 or 5 K, one sees a smeared steplike additional MR. The field at which this step occurs scales inversely with the square root of the magnetic field, and is related to the flux quantum through the wire. This effect has been attributed to localization, and is discussed elsewhere.⁴ Figures 10 and 11 show the temperature dependence of the magnetoresistance coefficient (1) in the longitudinal and transverse direction, respectively. The low temperature ($T < 10 \text{ K}$) data are dominated by the additional MR due to the localization effects,⁴ which increases as the temperature is decreased. In the temperature range $10 \text{ K} < T < 300 \text{ K}$, the temperature dependence of the longitudinal MR coefficient has been used¹³ to identify the semimetal-to-semiconductor transition which is calculated to occur as the wire diameter decreases below about 65 nm. The temperature dependence of the longitudinal MR of the 200- and 70-nm wires shows a maximum, which was also observed in the 109-nm sample of Ref. 13. This is consistent with the semimetallic nature of the wires:¹³ multiple electron pockets are occupied and thermally induced transfer of carriers between heavy and light electron pockets results in an increase in MR at lower temperature. At higher temperature, the increase in phonon scattering decreases the mobility and the MR. As the diameter is decreased to 48 nm or lower, the samples become semiconductors with only one electron pocket occupied, and the magnetoresistance is monotonically decreasing due to the decrease in mobility. The temperature dependence of the transverse MR coefficient, Fig. 11, also shows the effect of localization at $d < 40 \text{ nm}$ and $T < 10 \text{ K}$, while the high-temperature behavior is not clearly understood at this time.

SUMMARY AND ACKNOWLEDGEMENTS

In summary, we describe here a technique to prepare single-crystal manometer wires of Bi in anodic alumina. It circumvents the limitation of the high-pressure liquid technique used previously, and allows preparation of smaller diameter wires. We report the temperature and field dependence of the resistance, longitudinal and transverse magnetoresistance of Bi nanowires with diameters down to 7 nm, an order of magnitude smaller than Bi nanowires reported to date. The results are shown to be consistent with the theoretical band structure model that predict a semimetal-

to-semiconductor transition as the wire diameter is decreased below about 65 nm.

ACKNOWLEDGMENTS

The authors acknowledge very valuable discussion with Dr. G. Dresselhaus. The MIT authors received support from the National Science Foundation through Grant Nos. CTS-9257223 and DMR-9400334, the US Navy through Contract No. N00167-98-K-0024, and the ONR through the MURI Subcontract No. 0205-G-7A114-01 through UCLA.

-
- ¹D. A. Glocker and M. J. Skove, *Phys. Rev. B* **15**, 608 (1977).
²R. Hartman, *Phys. Rev.* **181**, 1070 (1969); J. E. Aubrey and C. J. Creasey, *J. Phys. F: Met. Phys.* **6**, L181 (1976); N. Garcia and Y. H. Kao, *Phys. Lett. A* **26**, 373 (1968); A. N. Friedmann and S. H. Koenig, *IBM J. Res. Dev.* **4**, 1958 (1960).
³V. S. Tsoi, *Pis'ma Zh. Eksp. Teor. Fiz.* **19**, 114 (1974) [*JETP Lett.* **19**, 70 (1974)].
⁴J. Heremans, C. M. Thrush, Z. Zhang, X. Sun, M. S. Dresselhaus, J. Y. Ying, and D. T. Morelli, *Phys. Rev. B* **58**, R10 091 (1998).
⁵D. E. Beutler and N. Giordano, *Phys. Rev. B* **38**, 8 (1988).
⁶G. Dresselhaus, M. S. Dresselhaus, Z. Zhang, X. Sun, J. Ying, and G. Chen, in *Proceedings of the XVIIth International Conference on Thermoelectrics, 1998, Nagoya, Japan*, edited by K. Koumoto (IEEE, Piscataway, NJ, 1998).
⁷J. Heremans and C. M. Thrush, *Phys. Rev. B* **59**, 12 579 (1999).
⁸M. Gurvitch, *J. Low Temp. Phys.* **38**, 777 (1980).
⁹N. B. Brandt, D. V. Gitsu, A. A. Nikolaeva, and Ya. G. Ponomarev, *Zh. Eksp. Teor. Fiz.* **72**, 2332 (1977) [*Sov. Phys. JETP* **45**, 1226 (1977)].
¹⁰R. G. Chambers, *Proc. R. Soc. London, Ser. A* **202**, 378 (1950).
¹¹N. B. Brandt, D. B. Gitsu, V. A. Dolma and Ya. G. Ponomarev, *Zh. Eksp. Teor. Fiz.* **92**, 913 (1987) [*Sov. Phys. JETP* **65**, 515 (1987)].
¹²R. B. Dingle, *Proc. R. Soc. London, Ser. A* **212**, 38 (1952).
¹³Z. Zhang, X. Sun, M. S. Dresselhaus, J. Y. Ying, and J. P. Heremans, *Appl. Phys. Lett.* **73**, 1589 (1998).
¹⁴Z. Zhang, J. Y. Ying, and M. S. Dresselhaus, *J. Mater. Res.* **13**, 1745 (1998).
¹⁵J-P. Michenaud and J-P. Issi, *J. Phys. C* **5**, 3061 (1972).
¹⁶O. P. Hansen and I. F. I. Mikhail, *Phys. Status Solidi B* **126**, 721 (1984).
¹⁷J. Heremans and O. P. Hansen, *J. Phys. C* **12**, 3483 (1979).
¹⁸M. P. Vecchi and M. S. Dresselhaus, *Phys. Rev. B* **10**, 771 (1974).